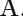
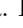
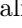



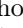
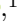


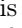
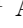
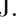
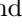

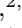
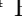

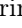











SPT-3G D1: Axion Early Dark Energy with CMB experiments and DESI

A. R. Khalife ¹ L. Balkenhol ¹ E. Camphuis ¹ A. J. Anderson ^{2,3,4} B. Ansarinejad,⁵ M. Archipley ^{4,3}
P. S. Barry ⁶ K. Benabed,¹ A. N. Bender ^{7,3,4} B. A. Benson ^{2,3,4} F. Bianchini ^{8,9,10} L. E. Bleem ^{7,3,4}
F. R. Bouchet ¹ L. Bryant,¹¹ M. G. Campitiello,⁷ J. E. Carlstrom ^{3,11,12,7,4} C. L. Chang,^{7,3,4}
P. Chaubal,⁵ P. M. Chichura ^{12,3} A. Chokshi,⁴ T.-L. Chou ^{4,3,13} A. Coerver,¹⁴ T. M. Crawford ^{4,3}
C. Daley ^{15,16} T. de Haan,¹⁷ K. R. Dibert,^{4,3} M. A. Dobbs,^{18,19} M. Doohan,⁵ A. Doussot,¹ D. Dutcher ²⁰
W. Everett,²¹ C. Feng,²² K. R. Ferguson ^{23,24} K. Fichman,^{12,3} A. Foster ²⁰ S. Galli,¹ A. E. Gambrel,³
R. W. Gardner,¹¹ F. Ge,^{8,9,25} N. Goeckner-Wald,^{9,8} R. Gualtieri ^{7,26} F. Guidi ¹ S. Guns,¹⁴
N. W. Halverson,^{27,28} E. Hivon ¹ W. L. Holzapfel,¹⁴ J. C. Hood,³ A. Hryciuk,^{12,3} N. Huang ¹⁴
F. K  r  zor  ,⁷ L. Knox,²⁵ M. Korman,²⁹ K. Korneelje,^{4,3,7} C.-L. Kuo,^{8,9,10} K. Levy,⁵ A. E. Lowitz ³ C. Lu,²²
G. P. Lynch ²⁵ A. Maniyar,^{8,9,10} E. S. Martsen,^{4,3} F. Menanteau,^{16,30} M. Millea ¹⁴ J. Montgomery,¹⁸
Y. Nakato,⁹ T. Natoli,³ G. I. Noble ^{31,32} Y. Omori,^{4,3} A. Ouellette,²² Z. Pan ^{7,3,12} P. Paschos,¹¹
K. A. Phadke ^{16,30,33} A. W. Pollak,⁴ K. Prabhu,²⁵ W. Quan,^{7,12,3} M. Rahimi,⁵ A. Rahlin ^{4,3}
C. L. Reichardt ⁵ M. Rouble,¹⁸ J. E. Ruhl,²⁹ E. Schiappucci,⁵ A. Simpson,^{4,3} J. A. Sobrin ^{2,3}
A. A. Stark,³⁴ J. Stephen,¹¹ C. Tandoi,¹⁶ B. Thorne,²⁵ C. Trendafilova,³⁰ C. Umilta ²² J. D. Vieira ^{16,22,30}
A. Vitrier ¹ Y. Wan,^{16,30} N. Whitehorn ²⁴ W. L. K. Wu ^{8,10} M. R. Young,^{2,3} and J. A. Zebrowski^{3,4,2}
(SPT-3G Collaboration)

¹*Sorbonne Universit  , CNRS, UMR 7095, Institut d'Astrophysique de Paris, 98 bis bd Arago, 75014 Paris, France*

²*Fermi National Accelerator Laboratory, MS209, P.O. Box 500, Batavia, IL, 60510, USA*

³*Kavli Institute for Cosmological Physics, University of Chicago,
5640 South Ellis Avenue, Chicago, IL, 60637, USA*

⁴*Department of Astronomy and Astrophysics, University of Chicago,
5640 South Ellis Avenue, Chicago, IL, 60637, USA*

⁵*School of Physics, University of Melbourne, Parkville, VIC 3010, Australia*

⁶*School of Physics and Astronomy, Cardiff University, Cardiff, CF24 3AA, UK*

⁷*High-Energy Physics Division, Argonne National Laboratory,
9700 South Cass Avenue, Lemont, IL, 60439, USA*

⁸*Kavli Institute for Particle Astrophysics and Cosmology,
Stanford University, 452 Lomita Mall, Stanford, CA, 94305, USA*

⁹*Department of Physics, Stanford University, 382 Via Pueblo Mall, Stanford, CA, 94305, USA*

¹⁰*SLAC National Accelerator Laboratory, 2575 Sand Hill Road, Menlo Park, CA, 94025, USA*

¹¹*Enrico Fermi Institute, University of Chicago, 5640 South Ellis Avenue, Chicago, IL, 60637, USA*

¹²*Department of Physics, University of Chicago,
5640 South Ellis Avenue, Chicago, IL, 60637, USA*

¹³*National Taiwan University, No. 1, Sec. 4, Roosevelt Road, Taipei 106319, Taiwan*

¹⁴*Department of Physics, University of California, Berkeley, CA, 94720, USA*

¹⁵*Universit   Paris-Saclay, Universit   Paris Cit  ,
CEA, CNRS, AIM, 91191, Gif-sur-Yvette, France*

¹⁶*Department of Astronomy, University of Illinois Urbana-Champaign,
1002 West Green Street, Urbana, IL, 61801, USA*

¹⁷*High Energy Accelerator Research Organization (KEK), Tsukuba, Ibaraki 305-0801, Japan*

¹⁸*Department of Physics and McGill Space Institute, McGill University,
3600 Rue University, Montreal, Quebec H3A 2T8, Canada*

¹⁹*Canadian Institute for Advanced Research, CIFAR Program in
Gravity and the Extreme Universe, Toronto, ON, M5G 1Z8, Canada*

²⁰*Joseph Henry Laboratories of Physics, Jadwin Hall,
Princeton University, Princeton, NJ 08544, USA*

²¹*Department of Astrophysical and Planetary Sciences,
University of Colorado, Boulder, CO, 80309, USA*

²²*Department of Physics, University of Illinois Urbana-Champaign,
1110 West Green Street, Urbana, IL, 61801, USA*

²³*Department of Physics and Astronomy, University of Los Angeles, CA, 90095, USA*

²⁴*Department of Physics and Astronomy, Michigan State University, East Lansing, MI 48824, USA*

²⁵*Department of Physics & Astronomy, University of California, One Shields Avenue, Davis, CA 95616, USA*

²⁶*Department of Physics and Astronomy, Northwestern University, 633 Clark St, Evanston, IL, 60208, USA*

²⁷*CASA, Department of Astrophysical and Planetary Sciences,
University of Colorado, Boulder, CO, 80309, USA*

²⁸*Department of Physics, University of Colorado, Boulder, CO, 80309, USA*

²⁹*Department of Physics, Case Western Reserve University, Cleveland, OH, 44106, USA*

³⁰Center for AstroPhysical Surveys, National Center for Supercomputing Applications, Urbana, IL, 61801, USA

³¹Dunlap Institute for Astronomy & Astrophysics, University of Toronto,
50 St. George Street, Toronto, ON, M5S 3H4, Canada

³²David A. Dunlap Department of Astronomy & Astrophysics,
University of Toronto, 50 St. George Street, Toronto, ON, M5S 3H4, Canada

³³NSF-Simons AI Institute for the Sky (SkAI), 172 E. Chestnut St., Chicago, IL 60611, USA

³⁴Center for Astrophysics | Harvard & Smithsonian,
60 Garden Street, Cambridge, MA, 02138, USA

(Dated: August 1, 2025)

We present the most up-to-date constraints on axion early dark energy (AEDE) from cosmic microwave background (CMB) and baryon acoustic oscillation (BAO) measurements. In particular, we assess the impact of data from ground-based CMB experiments, the South Pole Telescope (SPT) and the Atacama Cosmology Telescope (ACT)—both with and without *Planck*—on constraints on AEDE. We also highlight the impact that BAO information from the Dark Energy Spectroscopic Instrument (DESI) has on these constraints. From CMB data alone, we do not find statistically significant evidence for the presence of AEDE, and we find only moderate reduction in the Hubble tension. From the latest SPT data alone, we find the maximal fractional contribution of AEDE to the cosmic energy budget is $f_{\text{EDE}} < 0.12$ at 95% confidence level (CL), and the Hubble tension between the SPT and SH0ES results is reduced to the 2.3σ level. When combining the latest SPT, ACT, and *Planck* datasets, we find $f_{\text{EDE}} < 0.091$ at 95% CL and the Hubble tension at the 3.3σ level. In contrast, adding DESI data to the CMB datasets results in mild preference for AEDE and, in some cases, non-negligible reduction in the Hubble tension. From SPT+DESI, we find $f_{\text{EDE}} = 0.081^{+0.037}_{-0.052}$ at 68% CL, and the Hubble tension reduces to 1.5σ . From the combination of DESI with all three CMB experiments, we get $f_{\text{EDE}} = 0.071^{+0.035}_{-0.038}$ at 68% CL and a weak preference for AEDE over Λ CDM. This data combination, in turn, reduces the Hubble tension to 2.3σ . We highlight that this shift in parameters when adding the DESI dataset is a manifestation of the discrepancy currently present between DESI and CMB experiments in the concordance model Λ CDM.

I. INTRODUCTION

In recent months, three major datasets have been released that provide significant new constraints on cosmological parameters. These are SPT-3G’s observations of the Main field taken during 2019 and 2020 (SPT-3G D1) [1, 2, W. Quan et al., in preparation], the Atacama Cosmology Telescope’s sixth data release (ACT-DR6) [3–5], and the second release of the Dark Energy Spectroscopic Instrument (DESI-DR2) [6, 7]. SPT-3G D1 is the first in a series of SPT releases; following releases will improve the constraints even further [8]. With this trio of datasets, the time is auspicious to revisit one of the most promising models to ease the Hubble tension: Axion Early Dark Energy (AEDE) [9–12].

As a reminder, the Hubble tension is a discrepancy between cosmological model-dependent inferences of the expansion rate today, H_0 , and those using the classical distance ladder [13–20]. The latter method more directly determines H_0 and is much less sensitive to cosmological model assumptions. The most precise model-dependent inference of H_0 comes from the CMB. Within Λ CDM, the combination of SPT-3G D1, ACT-DR6, and *Planck*

results in $H_0 = 67.23 \pm 0.35$ km/s/Mpc [1].¹ The most precise result using the classical distance ladder is from the “Supernovae, H0, for the Equation of State of Dark energy” (SH0ES) collaboration, which finds $H_0 = 73.17 \pm 0.86$ km/s/Mpc [23]. This value is discrepant with the CMB one mentioned above by 6.4σ [1]. The quest to solve this tension has resulted in a plentitude of theoretical models [20, 24], of which AEDE is one of the most promising solutions. It is therefore interesting to update constraints on this model with the new datasets and see whether it still relieves the Hubble tension.

In this work, which is a follow-up to the cosmological constraints in [1], we present constraints on AEDE from the datasets mentioned above. We highlight the improvement in constraints due to the addition of SPT-3G D1 and ACT-DR6 to *Planck* data, and contrast constraints coming from the CMB alone to those with BAO data from DESI-DR2. In Section II, we present a concise description of the model, our assessment criteria for the ability of AEDE to solve the Hubble tension, and the numerical setup. We list the different datasets considered in this work in Section III. This Section is followed by a presentation of our main results and their implications for the status of AEDE from CMB data

¹ Each dataset contains $TT/TE/EE$ data and their corresponding lensing likelihood: [2] for SPT-3G D1, [21] for ACT-DR6, and [22] for *Planck* (see [1] for a detailed description of the datasets).

alone (Section IV A) and in combination with DESI-DR2 BAO data (Section IV B). We end with some concluding remarks in Section V.

II. EARLY DARK ENERGY: A BRIEF OVERVIEW

Early dark energy (EDE) models are motivated by higher-dimensional theories (e.g. String Theory) that predict the existence of scalar fields [25] and have been considered in many works prior to the appearance of the Hubble tension [26–28]. At the background level, the presence of such scalar fields can add to the energy budget of the Universe prior to recombination, increasing the Hubble parameter at that epoch, $H(z)$. This in turn decreases the sound horizon in a way that could compensate for the increase in H_0 needed to solve the Hubble tension [e.g. 29]. Moreover, the presence of such a field has additional non-trivial impacts on the dynamics of the Universe. For instance, the amount of energy density carried by the field changes the damping scale of the CMB, the amplitude of the Sachs-Wolfe effect [30] (including the early integrated one), the evolution of matter perturbations, and the “radiation driving” of acoustic oscillation amplitudes [31] (see [12] for more details).

Several EDE models have been proposed, each involving different mechanisms (see [11, 32–38] for more details). One particular model that captures a great deal of phenomenology with a fairly simple prescription is AEDE [11, 39–41], where an axion field (ϕ) causes the above-mentioned effects of EDE, with a potential

$$V(\phi) = m^2 f^2 [1 - \cos(\theta)]^n, \quad (1)$$

where m is the field’s mass, f is its decay constant, n is an integer, and $\theta = \phi/f$. The initial value of the latter, θ_i , is a free parameter of the model. Following previous works [20, 24, 37, 42–44], we consider the case² $n = 3$ and substitute m and f with the phenomenological parameters z_c and f_{EDE} [11, 39]. The former is the critical redshift at which ϕ becomes dynamical and its energy density decays faster than that of radiation, while the latter,

$$f_{\text{EDE}} = \frac{\rho_{\text{EDE}}(z)}{3H(z)^2/8\pi G} \Big|_{z=z_c}, \quad (2)$$

is the fraction of energy density occupied by the axion field at z_c .³ To solve the Hubble tension, one would

typically need $f_{\text{EDE}} \sim 10\%$ with z_c close to matter-radiation equality, i.e. $z_c \sim 10^3 - 10^4$ [11, 12].

To assess the ability of the model to solve the Hubble tension, we use three metrics: (1) marginalized posterior compatibility level, (2) difference of the maximum a posteriori, and (3) Akaike information criterion.

Marginalized Posterior Compatibility Level (MPCL): this metric, denoted hereafter as Q_{MPCL} , is defined in [24] (see [45, 46] for more details). Briefly, this Bayesian statistic quantifies how much the inferred value of H_0 in AEDE with a given dataset deviates from the value measured by SH0ES without assuming Gaussianity of the posteriors. In other words, it is a generalization of the rule-of-thumb difference in mean introduced in [47]. We consider $Q_{\text{MPCL}} \leq 3\sigma$ (see [24] for the meaning of σ) to be a passing score for the model.

Difference of the Maximum A Posteriori (DMAP): this is a frequentist statistic that measures the change in the best-fit χ^2 for a given data combination, within a model, due to the addition of information from SH0ES. The advantage of considering this metric along with Q_{MPCL} is twofold. First, it measures the ability of the whole model to fit the data, rather than focusing on only one parameter (H_0 in our case). Second, since it is a frequentist quantity, it avoids biases that could be due to the choice of priors (see [20, 24] for more details). This statistic is defined as [47]

$$Q_{\text{DMAP}} = \sqrt{\chi_{w/\text{SH0ES}}^2 - \chi_{w/o\text{SH0ES}}^2}, \quad (3)$$

where $\chi_{w/\text{SH0ES}}^2$ ($\chi_{w/o\text{SH0ES}}^2$) corresponds to the minimum χ^2 value of AEDE for a given dataset with (without) SH0ES information. A value of $Q_{\text{DMAP}} \leq 3\sigma$ ⁴ is considered a passing value for the model with a given dataset.

Akaike Information Criterion (AIC): also a frequentist statistic, this metric computes the improvement in fit a model has compared to Λ CDM for a given dataset. Although it does not quantify the tension on H_0 with SH0ES, it gives important information when judging if the model is an acceptable solution to the tension. For the model at hand, it is defined as [49, 50]:

$$\Delta\text{AIC} = \chi_{\text{AEDE}}^2 - \chi_{\Lambda\text{CDM}}^2 + 2N, \quad (4)$$

where χ_{AEDE}^2 ($\chi_{\Lambda\text{CDM}}^2$) is the minimum χ^2 of AEDE (Λ CDM) for a given dataset (which will be specified in Section IV) and N is the additional number of parameters that AEDE has relative to Λ CDM ($N = 3$ in this case). To pass this metric, we require $\Delta\text{AIC} \leq -6.91$, which corresponds to more than a “weak preference” on the Jeffreys scale [20, 51, 52]. Note that this metric has

² As shown in the works cited above, the case $n = 3$ is the most promising in easing the tension. This is partially attributed to the fact that in this case ϕ dilutes faster than radiation after it becomes dynamical, as opposed to the case $n = 2$ ($n = 1$), where ϕ dilutes as radiation (matter) [11, 39].

³ In units where the reduced Planck constant, \hbar , and the speed of light, c , are 1. We are also considering a spatially flat universe.

⁴ The number of σ s for this metric corresponds to the gaussian equivalent of a probability to exceed (PTE) from a $\Delta\chi^2$ for a χ^2 -distribution with 1 degree of freedom [47, 48].

been used in previous works for datasets that include SH0ES [20, 24]. However, we focus here on the ability of the model to fit the data without SH0ES. This focuses us on what we think is the more interesting question: is there SH0ES-independent evidence for the AEDE model?

If AEDE passes all three tests, we consider it as a viable solution to the Hubble tension. Although this set of metrics is not complete, it gives a reasonable indication of how well the model reduces the tension and fits the current datasets.

However, it is important to note that this model suffers from prior volume effects [33, 53]. As $f_{\text{EDE}} \rightarrow 0$, the model effectively becomes Λ CDM. When performing a Markov Chain Monte Carlo (MCMC), this limit could be reached for a large range of values for the additional parameters (θ_i and z_c). This will result in additional weight on that parameter space, and thus shift the samples' distribution of the MCMC towards the Λ CDM region. Another complication arises due to the choice of the prior on z_c . If the chosen prior range is higher than the recombination redshift, this will result in higher values of f_{EDE} but without significant change in H_0 [54]. Avoiding these prior-related effects motivates the use of the prior-independent, i.e. frequentist, statistics such as Q_{DMAP} or ΔAIC we use here. To determine a confidence interval that is not affected by this effect, one would need to perform a profile likelihood analysis and compute these intervals with techniques such as in [55]. Such an analysis is beyond the scope of the current work, but will be considered in future constraints on this model [Jhaveri et al, in preparation].

A. Numerical setup

We use the implementation of the AEDE model in the Boltzmann code AxiCLASS [39, 56]⁵, a modified version of CLASS [57, 58]. We impose uniform priors on the parameters of the model:

$$\begin{aligned} f_{\text{EDE}} &\sim \mathcal{U}(0, 0.5), \\ \theta_i &\sim \mathcal{U}(0.01, 3.1), \text{ and} \\ \log_{10}(a_c) &\sim \mathcal{U}(-4.5, -2.8), \end{aligned} \quad (5)$$

where a_c is the scale factor at z_c and $\mathcal{U}(a, b)$ denotes a uniform distribution between a and b . We also apply uniform priors on all of our sampled parameters (except the optical depth to reionization τ_{reio} , see Section III). We perform MCMC analysis with Cobaya [59–61], using the Metropolis-Hastings algorithm [62, 63], and consider chains to be converged when the Gelman-Rubin [64] statistic $R - 1 \sim 0.05$. When finding the best fit of the

model for a given data combination, we use the BOBYQA algorithm [65, 66] implemented in Cobaya. In order to speed up the inference process, we use the emulator OLE [67]⁶, but we report final results from regular MCMC runs that used CLASS only.

III. DATASETS

For the CMB, we use different combinations of SPT-3G D1, ACT-DR6, and *Planck* data in primary CMB and lensing. We consider constraints from SPT-3G D1 alone and in combination with ACT-DR6 (SPT+ACT), and we consider SPT+ACT in combination with *Planck* (CMB-SPA). We also combine each of these data combinations with BAO data from DESI-DR2 (DESI). We list the different datasets involved in this work, following the setup of [1], in Table I.

In all the different combinations, we substitute the low- ℓ EE information from *Planck* with a prior on τ_{reio} from the findings of [68]. This is a Gaussian with a mean value of 0.051 and a standard deviation of 0.006, i.e. $\tau_{\text{reio}} \sim \mathcal{N}(0.051, 0.006)$. Moreover, we use the CMB-only versions of the likelihoods, known as *lite*, for the SPT-3G D1 (SPTlite) [69] and ACT-DR6 data (ACT-lite), while we use *clipy* [70] for the *Planck* dataset. When combining *Planck* and ACT-DR6, we follow the prescription described in [4, 5] and cut the *Planck* TT spectrum at $\ell > 1000$, while $\ell > 600$ is cut for the TE and EE spectra. This combination, along with the lensing likelihood of each dataset, is labeled P-ACT-L. The packages associated with each dataset are listed in Table III.

We consider CMB-SPA as our CMB-only baseline, and CMB-SPA + DESI as the one in combination with BAO. We compute Q_{DMAP} and ΔAIC for these two data combinations, and use them to assess the performance of AEDE.⁷ When computing Q_{DMAP} , we incorporate data from SH0ES as a Gaussian likelihood: $H_0 \sim \mathcal{N}(73.17, 0.86)$.

IV. RESULTS

In this section, we present our main results, starting with constraints from CMB datasets and then in combination with DESI.

⁵ <https://github.com/PoulinV/AxiCLASS>. Note that we used version v3.2.0 of the code, with the precision parameters set as described in Appendix A of [5].

⁶ <https://github.com/svenguenter/OLE>

⁷ In principle, one can compute Q_{DMAP} and ΔAIC for SPT-3G D1 and SPT+ACT. However, since computing these statistics is computationally expensive, and given that SPT-3G D1 and SPT+ACT are subsets of CMB-SPA and CMB-SPA+DESI, it would add little extra information to assess the model based on Q_{DMAP} and ΔAIC for such subsets.

Name	dataset
SPT-3G D1	SPT-3G D1 $TT/TE/EE$ CMB spectra [1] + CMB lensing spectrum [2].
<i>Planck</i>	Planck 2018 high- ℓ $TT/TE/EE$ and low- ℓ TT spectra (PR3) [71, 72] + NPIPE PR4 CMB lensing spectrum [73].
ACT-DR6	ACT-DR6 $TT/TE/EE$ CMB spectra [5, 74] + ACT-DR6 CMB lensing spectrum [75, 76].
P-ACT-L	The combination of ACT-DR6 and <i>Planck</i> with the appropriate ℓ -cuts for the latter: the TT spectrum cut at $\ell > 1000$, while the TE and EE spectra cut at $\ell > 600$ + ACT-DR6 CMB lensing spectrum + NPIPE PR4 CMB lensing spectrum.
SPT+ACT	SPT-3G D1 + ACT-DR6.
CMB-SPA	SPT-3G D1 + P-ACT-L.
DESI	DESI-DR2 BAO data [6].

TABLE I. Summary of datasets used in this work.

A. Constraints from CMB data alone

We show our constraints from CMB datasets in the top plot of Fig. 1⁸ and the upper part of Table II. In addition to H_0 and f_{EDE} , we present constraints on the matter density parameter, Ω_m , and the sound horizon at the baryonic drag epoch [77, 78], r_d , multiplied by $h = H_0/(100 \text{ km/s/Mpc})$.

From CMB data alone, we first find that different CMB data combinations are consistent with each other in this model space to within $\sim 0.4\sigma$. Following [1], we check for the consistency between two datasets by computing $\chi^2 = \Delta p^T \Sigma^{-1} \Delta p$ (Δp is the difference between the means of a parameter p from two datasets, Σ^{-1} is the inverse of the sum of the covariance matrices and T stands for transpose), from which we compute its PTE and then obtain the corresponding one-dimensional Gaussian fluctuation. This computation is done on the parameters set $\{H_0, \Omega_b h^2, \Omega_c h^2, n_s\}$. Here, Ω_b and Ω_c are the density parameters of baryons and dark matter, respectively, and n_s is the spectral index of the primordial power spectrum.

The upper limit on f_{EDE} at 95% confidence level (CL) from SPT-3G D1 ($f_{\text{EDE}} < 0.12$) is almost twice the corresponding *Planck* one ($f_{\text{EDE}} < 0.077$), while the SPT+ACT constraint ($f_{\text{EDE}} < 0.068$) is 12% smaller

than *Planck*'s.⁹ Furthermore, all datasets appearing in Fig. 1 are consistent with $f_{\text{EDE}} = 0$ at less than 68% CL. With CMB-SPA, we get the most up-to-date constraint on f_{EDE} from the CMB alone, $f_{\text{EDE}} < 0.091$.¹⁰

To evaluate the impact of adding SPT data on the constraints, specifically those from the P-ACT combination of [5], we consider constraints from CMB-SPA without including lensing information from any of the three datasets. The addition of SPT-3G D1 (without lensing) to the P-ACT dataset reduces the upper limit from $f_{\text{EDE}} < 0.12$ [5] to $f_{\text{EDE}} < 0.10$, a 16% improvement in constraints. Note that in this comparison we used the `sroll2` prior on τ_{reio} [80] in accordance with the P-ACT dataset of [5].

Finally, as can be seen from Table II, the Hubble tension gets reduced to 2.3σ and 2.9σ for SPT-3G D1 and SPT+ACT, respectively, using Q_{MPCL} , compared to 6.2σ and 6.7σ in ΛCDM , respectively, found in [1]. However, with the CMB only baseline dataset, CMB-SPA, the tension is still present, albeit reduced from 6.4σ in the ΛCDM case to 3.3σ for this model. On the other hand, we find $Q_{\text{DMAP}} = 2.6\sigma$, which passes our threshold for this test. Moreover, comparing the best-fit χ^2 between this model and ΛCDM ($\Delta\chi^2 = \chi_{\text{AEDE}}^2 - \chi_{\Lambda\text{CDM}}^2$), we find a $\Delta\chi^2 = -4.4$ improvement in the best fit with the CMB-SPA dataset. This corresponds to $\Delta\text{AIC} = 1.6$, which does not pass our threshold.

Therefore, out of the three metrics used here to assess the performance of AEDE (Q_{MPCL} , Q_{DMAP} , and ΔAIC), we find that it passes only one of them (Q_{DMAP}). This means that, from CMB data alone, AEDE cannot be considered as a solution to the Hubble tension.

B. Constraints from CMB and BAO data

We now consider the impact of DESI data on AEDE, with the results shown in the bottom plot of Fig. 1 and the lower part of Table II. We first assess the consistency between CMB and DESI data by comparing the constraints in the Ω_m - hr_d plane between each CMB dataset mentioned above and DESI.¹¹ We find the consistency between SPT-3G D1, SPT+ACT, and CMB-SPA, with DESI at 1.5σ , 2.8σ , and 2.3σ , respectively, in AEDE, compared to 2.5σ , 3.7σ , and 2.8σ for ΛCDM [1]. Given that all three are below the 3σ

⁸ Although $R-1 \leq 0.05$ for all the MCMC runs appearing in this work, we made a further test of the convergence of these chains. We split the samples into two random sets (after removing the burn-in) and found that the constraints from each set match to an excellent degree.

⁹ We did not compare the constraints from SPT+ACT to those of the `CamSpec` likelihood based on *Planck* PR4 maps [79]. In that case, we expect SPT+ACT and `CamSpec` to give similar constraints.

¹⁰ Note that the increase in the upper limit going from SPT+ACT to CMB-SPA is due to including only large-scale information from *Planck*, which tends to shift the posteriors to higher values [12, 42, 44].

¹¹ We follow the criterion set in [1] and consider 3σ as the threshold for two datasets to be consistent (see Section VII.C in [1]).

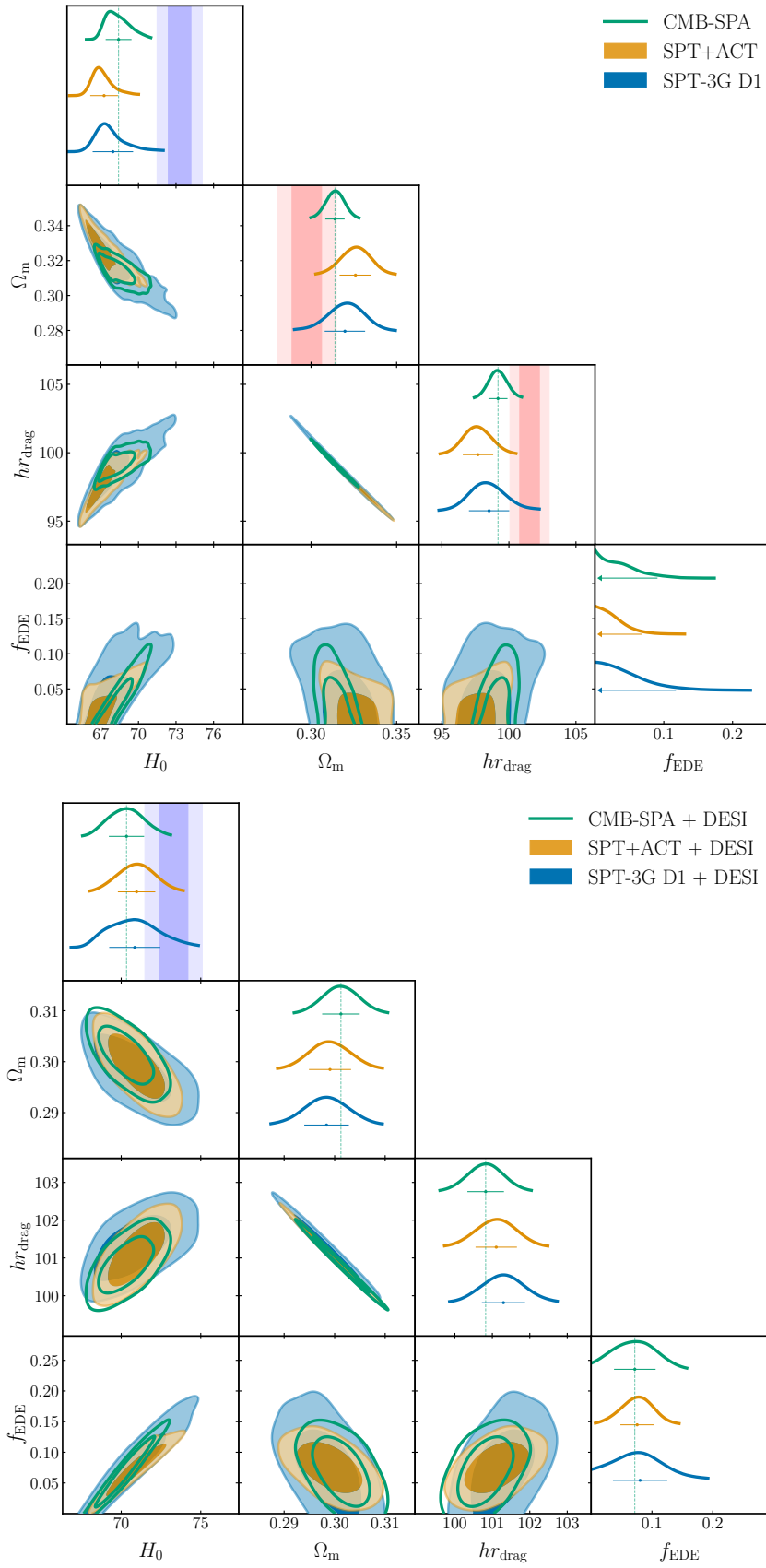


FIG. 1. *Top:* Constraints on the parameter set $\{H_0, \Omega_m, hr_d, f_{\text{EDE}}\}$ in the AEDE model from SPT-3G D1 in blue, SPT+ACT in orange, and CMB-SPA in green (see Table 1 for the definition of each dataset). The shaded purple band in the H_0 1D posterior corresponds to the SH0ES measurements [23], while the red bands appearing in the 1D posteriors of Ω_m and hr_d correspond to the DESI inferred values within ΛCDM [6]. *Bottom:* Same as the top plot, but with the inclusion of DESI data. From CMB data, we do not find any preference for EDE over ΛCDM and the Hubble tension remains, now at the 3.3σ level with CMB-SPA. On the other hand, adding DESI data reduces the tension to 2.3σ , yet there is still no strong statistical evidence for AEDE.

Parameter	SPT-3G D1	SPT+ACT	CMB-SPA
H_0 [km/s/Mpc]	$67.96^{+0.58}_{-1.7}$	$67.25^{+0.47}_{-1.1}$	$68.41^{+0.66}_{-1.3}$
Ω_m	$0.320^{+0.012}_{-0.010}$	0.3260 ± 0.0093	0.3140 ± 0.0056
hr_{drag} [Mpc]	$98.5^{+1.2}_{-1.6}$	$97.7^{+1.0}_{-1.2}$	$99.19^{+0.66}_{-0.72}$
f_{EDE}	< 0.12	< 0.068	< 0.091
$Q_{\text{MPCL}}[\sigma]$	2.3	2.9	3.3
$Q_{\text{DMAP}}[\sigma]$	---	---	2.6
ΔAIC	---	---	1.6

+ DESI

H_0 [km/s/Mpc]	$70.9^{+1.3}_{-1.9}$	71.0 ± 1.2	70.3 ± 1.1
Ω_m	0.2984 ± 0.0044	0.2991 ± 0.0042	0.3013 ± 0.0038
hr_{drag} [Mpc]	101.30 ± 0.58	101.10 ± 0.55	100.82 ± 0.49
f_{EDE}	$0.081^{+0.037}_{-0.052}$	$0.076^{+0.028}_{-0.027}$	$0.071^{+0.035}_{-0.038}$
	(0.16)	(0.12)	(0.13)
$Q_{\text{MPCL}}[\sigma]$	1.5	1.8	2.3
$Q_{\text{DMAP}}[\sigma]$	---	---	1.8
ΔAIC	---	---	-4.8

TABLE II. *Top:* CMB-only constraints on cosmological parameters for AEDE. For f_{EDE} , we present upper limits at the 95% CL. We also show Q_{MPCL} for every dataset, while we show the Q_{DMAP} (eq. 3) and ΔAIC (eq. 4) metrics for CMB-SPA. *Bottom:* Same as the top part but with the addition of DESI. For f_{EDE} , we show the mean and 68% CL and below them in parenthesis the one-tail upper limit at 95% CL.^a

^a We calculate the one-tail upper limit at 95% CL by integrating the posterior distribution from the boundary $f_{\text{EDE}} = 0$, in accordance with the 95% CL quoted in the top part of the Table.

threshold, we proceed to combine each CMB dataset with DESI.

When we include DESI data, the conclusions of the previous section change. First, as expected, the degeneracy of f_{EDE} with H_0 and $\Omega_c h^2$ (see Figs. 4 and 5), and the preference for lower (higher) $\Omega_m (hr_d)$ by DESI, shifts the constraints with the CMB datasets, rendering them in agreement with the Ω_m - hr_d constraints (within ΛCDM) from DESI (see bottom plot of Fig. 1). Second, we no longer have an upper limit on f_{EDE} , but rather a weak preference for $f_{\text{EDE}} > 0$, as can be seen from the lower part of Table II. These constraints deviate from $f_{\text{EDE}} = 0$ at 1.8σ , 2.8σ , and 1.9σ for SPT-3G D1, SPT+ACT, and CMB-SPA (each combined with DESI), respectively. Note that the increase in the error bar going from SPT+ACT to CMB-SPA seen in Table II is attributed to the highly non-gaussian distributions and the preference for different regions in the $(f_{\text{EDE}}, \theta_1)$ plane between the two data combinations (see Fig. 5). Third, the Hubble tension is now reduced below the 3σ threshold for all three CMB datasets when including DESI, with $Q_{\text{MPCL}} = 2.3\sigma$ for CMB-SPA + DESI. Furthermore, $Q_{\text{DMAP}} = 1.8\sigma$ for this model with CMB-SPA + DESI, and thus passes the threshold for it to be a better fit to the data when SH0ES information is included. Finally, the goodness of fit for this model is also improved compared to ΛCDM , with $\Delta\chi^2 = -10.8$ for CMB-SPA + DESI. This improvement is better than other Hubble tension solutions, such as the varying

electron mass in a non-flat geometry [81–84], which has $\Delta\chi^2 = -6.8$ (see Table VII of [1] for comparison with other models). However, the resultant ΔAIC for this model is $\Delta\text{AIC} = -4.8$, which corresponds to a weak preference for AEDE over ΛCDM and thus does not pass the threshold.

In summary, the addition of DESI to CMB data does ease the tension according to the Q_{MPCL} and Q_{DMAP} metrics. However, there is no strong statistical evidence to prefer this model over ΛCDM . Moreover, as pointed out by [85], adding Supernova Ia data from the Pantheon+ sample [86] to *Planck*, ACT-DR6 and DESI data results in an even weaker preference for this model and an inability to reduce the Hubble tension. It is important to point out that this shift in parameters for AEDE when including DESI data is another manifestation of the discrepancy that currently exists between CMB and DESI BAO data in ΛCDM .

As found in [1], the CMB-BAO discrepancy can be projected onto many extensions of ΛCDM , and AEDE is yet another example. To see this more clearly, we plot in Fig. 2 the 2D posterior of $(\Omega_m, \Omega_m(hr_d/147.1 \text{ Mpc})^2)$ for CMB-SPA and CMB-SPA + DESI, within EDE, and the posterior for DESI alone and CMB-SPA within ΛCDM . The reason for choosing $\Omega_m(hr_d/147.1 \text{ Mpc})^2$ instead of hr_d is twofold. First, it allows for a better visualization of the discrepancy, given the strong Ω_m - hr_d degeneracy, and second $\Omega_m(hr_d)^2$ is a combination which both the CMB and BAO data constrain well. From this plot, we can see how allowing f_{EDE} to take on non-zero values (roughly 4–10%) results in an overlap between the CMB-SPA- and DESI-preferred regions, thus reducing the discrepancy seen in ΛCDM . This explains why adding DESI data results in the shifts seen in Table II and an improvement in the fit compared to ΛCDM .

V. CONCLUSION

In this work, we extend the cosmological results of [1] to include constraints on the AEDE model. We focus on constraints from SPT-3G D1, SPT+ACT, and CMB-SPA. We also present constraints from adding DESI to each of these data combinations.

From CMB data alone, we find that all data combinations are statistically consistent with each other and do not show appreciable evidence for AEDE. The constraints on f_{EDE} coming from SPT+ACT are $\sim 12\%$ smaller than the ones from *Planck*. Moreover, with CMB-SPA, we find that the Hubble tension is still present at the 3.3σ level ($H_0 = 68.41^{+0.66}_{-1.3}$) with the upper limit on f_{EDE} at the 95% CL being $f_{\text{EDE}} < 0.091$, and the improvement in best fit for this case compared to ΛCDM is only $4.4 \chi^2$ points. While the Q_{DMAP} metric for this data combination passes our threshold at 2.6σ , on balance these results show that, for CMB data alone, AEDE is not able to solve the tension and does not show a strong statistical preference over ΛCDM .

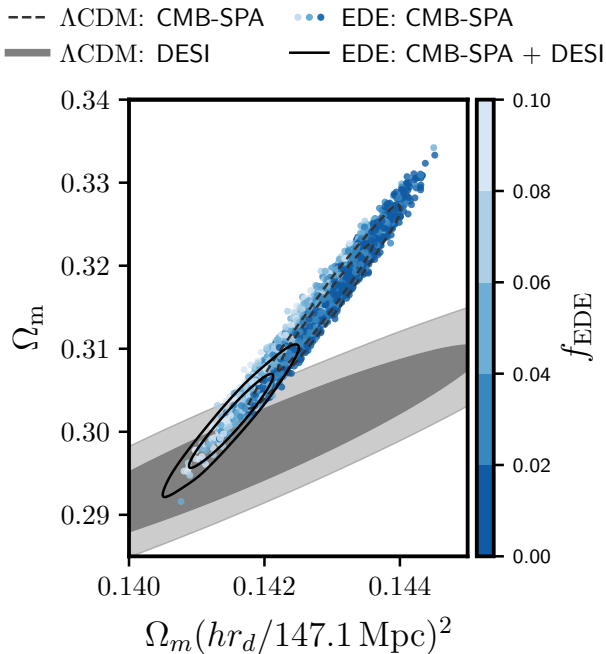


FIG. 2. Constraints in the $(\Omega_m, \Omega_m(hr_d/147.1 \text{ Mpc})^2)$ plane from CMB-SPA (blue dots) and CMB-SPA + DESI (solid black contours) for the AEDE model. Also shown are constraints from CMB-SPA (gray dashed contours) and DESI (gray solid contours) within ΛCDM . (Note that the DESI contours are identical in the AEDE case due to the insensitivity of the BAO data to this model's parameters.) The dots are colored according to the f_{EDE} values of the samples in the range $[0, 0.1]$. The discrepancy between CMB and DESI BAO data in ΛCDM projects onto a preference for higher values of f_{EDE} .

We also find that the discrepancy between SPT-3G D1, SPT+ACT, and CMB-SPA with DESI in the Ω_m - hr_d plane is reduced to 1.5σ , 2.8σ , and 2.3σ , respectively, for this model. With this level of agreement within the AEDE model, the two types of data can be sensibly combined.

Unlike the CMB-only case, adding BAO data from DESI results in a mild preference for $f_{\text{EDE}} > 0$ which, for CMB-SPA + DESI is $f_{\text{EDE}} = 0.071^{+0.035}_{-0.038}$, a deviation from $f_{\text{EDE}} = 0$ at 1.9σ . This preference is accompanied with an increase in H_0 to 70.3 ± 1.1 km/s/Mpc, which corresponds to a 2.3σ difference with the SH0ES measurement. With this data combination, the model also passes the $Q_{\text{DMAP}} < 3\sigma$ test, where we find $Q_{\text{DMAP}} = 1.8\sigma$. Moreover, with CMB-SPA + DESI, the best-fit χ^2 of this model improves by 10.3 compared to ΛCDM . However, this is not enough improvement for the model to pass the ΔAIC criterion ($\Delta\text{AIC} = -4.8$ for CMB-SPA + DESI); at best, the data indicate a weak preference for the AEDE model compared to ΛCDM . We show a summary of the main results in Fig. 3.

We point out that this shift in parameters seen when adding the DESI data is a manifestation of the currently existing discrepancy between DESI and CMB data in ΛCDM . With more precise data, such as that expected soon from further SPT releases [8], early observations with the Simons Observatory [87], or upcoming data from DESI we might be able to understand the origin of this discrepancy and whether it points to truly new physics or to unknown sources of systematic error.

VI. ACKNOWLEDGMENTS

The South Pole Telescope program is supported by the National Science Foundation (NSF) through awards OPP-1852617 and OPP-2332483. Partial support is also provided by the Kavli Institute of Cosmological Physics at the University of Chicago. Argonne National Laboratory's work was supported by the U.S. Department of Energy, Office of High Energy Physics, under contract DE-AC02-06CH11357. The UC Davis group acknowledges support from Michael and Ester Vaida. Work at the Fermi National Accelerator Laboratory (Fermilab), a U.S. Department of Energy, Office of Science, Office of High Energy Physics HEP User Facility, is managed by Fermi Forward Discovery Group, LLC, acting under Contract No. 89243024CSC000002. The Melbourne authors acknowledge support from the Australian Research Council's Discovery Project scheme (No. DP210102386). The Paris group has received funding from the European Research Council (ERC) under the European Union's Horizon 2020 research and innovation program (grant agreement No 101001897), and funding from the Centre National d'Etudes Spatiales. The SLAC group is supported in part by the Department of Energy at SLAC National Accelerator Laboratory, under contract DE-AC02-76SF00515. This work has made use of the Infinity Cluster hosted by Institut d'Astrophysique de Paris. We thank Stephane Rouberol for smoothly running this cluster for us. This work relied on the NumPy library for numerical computations [88], the SciPy library for scientific computing [89], and the Matplotlib library for plotting [90]. Posterior sampling analysis and plotting were performed using the GetDist package [91].

Appendix A: Additional Results

In this section, for completeness, we present constraints on the set of cosmological parameters $\{\Omega_b h^2, \Omega_c h^2, 100\theta_s, n_s, \log(10^{10} A_s), f_{\text{EDE}}, \log_{10} z_c, \theta_i\}$, where θ_s is the angular size of the sound horizon at recombination and A_s is the amplitude of the primordial spectrum. The constraints from CMB data only are shown in Fig. 4, and those from the combination of CMB and DESI BAO data are shown in Fig. 5.

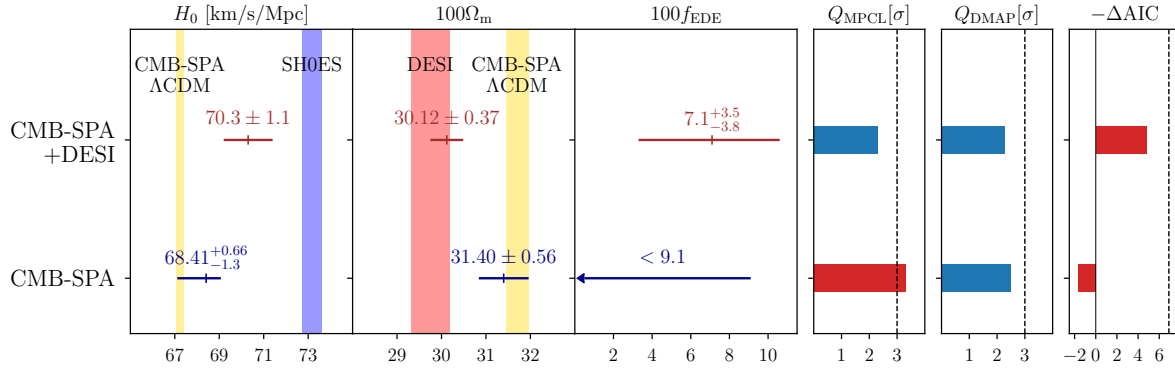


FIG. 3. Summary of the main results of this work. Shown are constraints, within AEDE, from CMB-SPA (in dark blue) and CMB-SPA + DESI (in brown) on H_0 (far left), $100\Omega_m$ (second to the left), and f_{EDE} (third to the left). In the H_0 panel, we show the 68% CL from SH0ES (purple band) and that of CMB-SPA within Λ CDM (gold band). In the $100\Omega_m$ panel, we show the 68% CL from DESI (red band) and that of CMB-SPA (gold band), both within Λ CDM. We also show the three metrics Q_{MPCL} (third to the right), Q_{DMAP} (second to the right), and $-\Delta AIC$ (far right). For each of these, we show their passing threshold as dashed lines (3σ , 3σ , and 6.91, respectively), and in blue the cases that pass these thresholds while in red those that do not. More details are presented in Table II.

Appendix B: Packages of datasets

-
- [1] Camphuis, E., et al. SPT-3G D1: CMB temperature and polarization power spectra and cosmology from 2019 and 2020 observations of the SPT-3G Main field. 2025. <https://arxiv.org/abs/2506.20707>
 - [2] Ge, F., et al. Cosmology from CMB lensing and delensed EE power spectra using 2019–2020 SPT-3G polarization data. 2025, Phys. Rev. D, 111, 083534, doi: [10.1103/PhysRevD.111.083534](https://arxiv.org/abs/2503.14451)
 - [3] Naess, S., et al. The Atacama Cosmology Telescope: DR6 Maps. 2025. <https://arxiv.org/abs/2503.14451>
 - [4] Louis, T., et al. The Atacama Cosmology Telescope: DR6 Power Spectra, Likelihoods and Λ CDM Parameters. 2025. <https://arxiv.org/abs/2503.14452>
 - [5] Calabrese, E., et al. The Atacama Cosmology Telescope: DR6 Constraints on Extended Cosmological Models. 2025. <https://arxiv.org/abs/2503.14454>
 - [6] Abdul Karim, M., et al. DESI DR2 Results II: Measurements of Baryon Acoustic Oscillations and Cosmological Constraints. 2025. <https://arxiv.org/abs/2503.14738>
 - [7] The Dark Energy Spectroscopic Instrument (DESI). 2019, in Bulletin of the American Astronomical Society, Vol. 51, 57. <https://arxiv.org/abs/1907.10688>
 - [8] Prabhu, K., et al. Testing the Λ CDM Cosmological Model with Forthcoming Measurements of the Cosmic Microwave Background with SPT-3G. 2024, Astrophys. J., 973, 4, doi: [10.3847/1538-4357/ad5ff1](https://arxiv.org/abs/2405.1538)
 - [9] Karwal, T., & Kamionkowski, M. Dark energy at early times, the Hubble parameter, and the string axiverse. 2016, Phys. Rev. D, 94, 103523, doi: [10.1103/PhysRevD.94.103523](https://arxiv.org/abs/1603.04468)
 - [10] Mörtzell, E., & Dhawan, S. Does the Hubble constant tension call for new physics? 2018, JCAP, 09, 025, doi: [10.1088/1475-7516/2018/09/025](https://arxiv.org/abs/1808.07431)
 - [11] Poulin, V., Smith, T. L., Karwal, T., & Kamionkowski, M. Early Dark Energy Can Resolve The Hubble Tension. 2019, Phys. Rev. Lett., 122, 221301, doi: [10.1103/PhysRevLett.122.221301](https://arxiv.org/abs/1907.08571)
 - [12] Poulin, V., Smith, T. L., & Karwal, T. The Ups and Downs of Early Dark Energy solutions to the Hubble tension: a review of models, hints and constraints circa 2023. 2023. <https://arxiv.org/abs/2302.09032>
 - [13] Abdalla, E., et al. Cosmology intertwined: A review of the particle physics, astrophysics, and cosmology associated with the cosmological tensions and anomalies. 2022, JHEAp, 34, 49, doi: [10.1016/j.jheap.2022.04.002](https://arxiv.org/abs/2208.08139)
 - [14] Di Valentino, E., Mena, O., Pan, S., Visinelli, L., Yang, W., Melchiorri, A., Mota, D. F., Riess, A. G., & Silk, J. In the realm of the Hubble tension—a review of solutions. 2021, Class. Quant. Grav., 38, 153001, doi: [10.1088/1361-6382/ac086d](https://arxiv.org/abs/2103.01550)
 - [15] Camarena, D., & Marra, V. Local determination of the Hubble constant and the deceleration parameter. 2020, Phys. Rev. Res., 2, 013028, doi: [10.1103/PhysRevResearch.2.013028](https://arxiv.org/abs/2005.08328)
 - [16] —. On the use of the local prior on the absolute magnitude of Type Ia supernovae in cosmological inference. 2021, Mon. Not. Roy. Astron. Soc., 504, 5164, doi: [10.1093/mnras/stab1200](https://arxiv.org/abs/2103.01550)
 - [17] Verde, L., Protopapas, P., & Jimenez, R. Planck and the local Universe: Quantifying the tension. 2013, Phys. Dark Univ., 2, 166, doi: [10.1016/j.dark.2013.09.002](https://arxiv.org/abs/1304.6877)
 - [18] Bernal, J. L., Verde, L., & Riess, A. G. The trouble with H_0 . 2016, JCAP, 10, 019, doi: [10.1088/1475-7516/2016/10/019](https://arxiv.org/abs/1605.01424)
 - [19] Verde, L., Treu, T., & Riess, A. G. Tensions between the

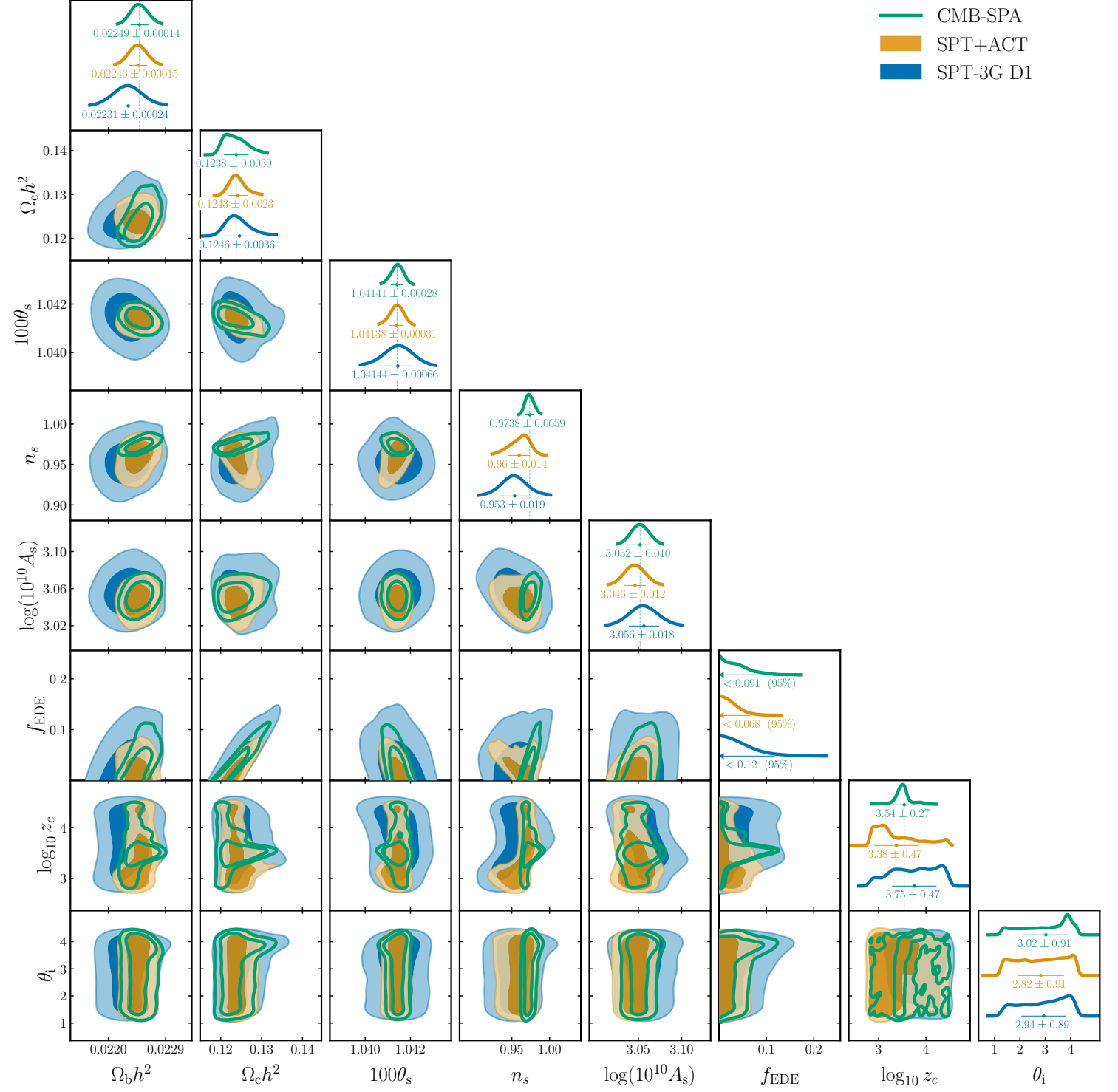


FIG. 4. Same as the top plot of Fig. 1 but for additional cosmological parameters. Below each 1D posterior, we show the mean and 68% CL of the parameter, except for f_{EDE} , where we show its upper limit at 95% CL.

early and late Universe. 2019, Nature Astronomy, 3, 891, doi: [10.1038/s41550-019-0902-0](https://doi.org/10.1038/s41550-019-0902-0)

- [20] Schöneberg, N., Franco Abellán, G., Pérez Sánchez, A., Witte, S. J., Poulin, V., & Lesgourgues, J. The H0 Olympics: A fair ranking of proposed models. 2022, Phys.

Rept., 984, 1, doi: [10.1016/j.physrep.2022.07.001](https://doi.org/10.1016/j.physrep.2022.07.001)

- [21] Madhavacheril, M. S., et al. The Atacama Cosmology Telescope: DR6 Gravitational Lensing Map and Cosmological Parameters. 2023. <https://arxiv.org/abs/2304.05203>

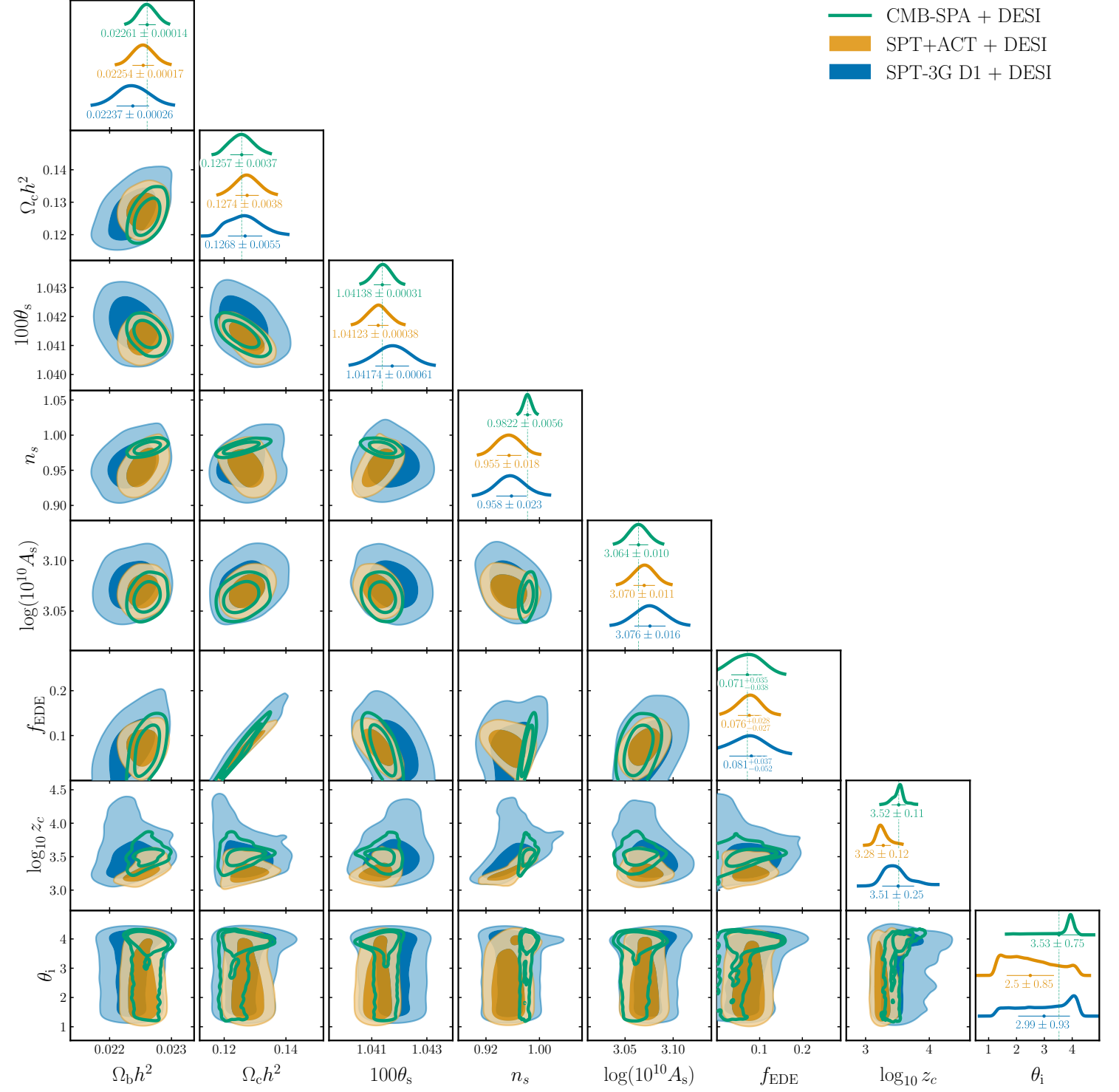


FIG. 5. Same as Fig. 4 but when including DESI data. For f_{EDE} , we show the mean and the 68% CL.

- [22] Carron, J., Mirmelstein, M., & Lewis, A. CMB lensing from Planck PR4 maps. 2022, JCAP, 09, 039, doi: [10.1088/1475-7516/2022/09/039](https://doi.org/10.1088/1475-7516/2022/09/039)
- [23] Breuval, L., Riess, A. G., Casertano, S., Yuan, W., Macri, L. M., Romaniello, M., Murakami, Y. S., Scolnic, D., Anand, G. S., & Soszyński, I. Small Magellanic Cloud

- Cepheids Observed with the Hubble Space Telescope Provide a New Anchor for the SH0ES Distance Ladder. 2024, Astrophys. J., 973, 30, doi: [10.3847/1538-4357/ad630e](https://doi.org/10.3847/1538-4357/ad630e)
- [24] Khalife, A. R., Zanjani, M. B., Galli, S., Günther, S., Lesgourgues, J., & Benabed, K. Review of Hubble

dataset	Link to Package
SPT-3G D1	https://pole.uchicago.edu/public/data/camphuis25/ https://github.com/SouthPoleTelescope/spt_candl_data https://pole.uchicago.edu/public/data/ge25/
<i>Planck</i>	https://github.com/benabed/clipy https://pla.esac.esa.int/ https://github.com/carronj/planck_PR4_lensing
ACT-DR6	https://github.com/ACTCollaboration/DR6-ACT-lite https://github.com/ACTCollaboration/act_dr6_lenslike

TABLE III. Likelihoods and their corresponding links.

- tension solutions with new SH0ES and SPT-3G data. 2024, JCAP, 04, 059, doi: [10.1088/1475-7516/2024/04/059](https://doi.org/10.1088/1475-7516/2024/04/059)
- [25] Kamionkowski, M., Pradler, J., & Walker, D. G. E. Dark energy from the string axiverse. 2014, Phys. Rev. Lett., 113, 251302, doi: [10.1103/PhysRevLett.113.251302](https://doi.org/10.1103/PhysRevLett.113.251302)
- [26] Doran, M., Lilley, M. J., Schwindt, J., & Wetterich, C. Quintessence and the separation of CMB peaks. 2001, Astrophys. J., 559, 501, doi: [10.1086/322253](https://doi.org/10.1086/322253)
- [27] Wetterich, C. Phenomenological parameterization of quintessence. 2004, Phys. Lett. B, 594, 17, doi: [10.1016/j.physletb.2004.05.008](https://doi.org/10.1016/j.physletb.2004.05.008)
- [28] Doran, M., & Robbers, G. Early dark energy cosmologies. 2006, JCAP, 06, 026, doi: [10.1088/1475-7516/2006/06/026](https://doi.org/10.1088/1475-7516/2006/06/026)
- [29] Knox, L., & Millea, M. Hubble constant hunter's guide. 2020, Phys. Rev. D, 101, 043533, doi: [10.1103/PhysRevD.101.043533](https://doi.org/10.1103/PhysRevD.101.043533)
- [30] Sachs, R. K., & Wolfe, A. M. Perturbations of a Cosmological Model and Angular Variations of the Microwave Background. 1967, The Astrophysical Journal, 147, 73, doi: [10.1086/148982](https://doi.org/10.1086/148982)
- [31] Hu, W., & White, M. J. The Damping tail of CMB anisotropies. 1997, Astrophys. J., 479, 568, doi: [10.1086/303928](https://doi.org/10.1086/303928)
- [32] Niedermann, F., & Sloth, M. S. Resolving the Hubble tension with new early dark energy. 2020, Phys. Rev. D, 102, 063527, doi: [10.1103/PhysRevD.102.063527](https://doi.org/10.1103/PhysRevD.102.063527)
- [33] Herold, L., Ferreira, E. G. M., & Komatsu, E. New Constraint on Early Dark Energy from Planck and BOSS Data Using the Profile Likelihood. 2022, Astrophys. J. Lett., 929, L16, doi: [10.3847/2041-8213/ac63a3](https://doi.org/10.3847/2041-8213/ac63a3)
- [34] Herold, L., & Ferreira, E. G. M. Resolving the Hubble tension with Early Dark Energy. 2022, <https://arxiv.org/abs/2210.16296>
- [35] Murai, K., Naokawa, F., Namikawa, T., & Komatsu, E. Isotropic cosmic birefringence from early dark energy. 2023, Phys. Rev. D, 107, L041302, doi: [10.1103/PhysRevD.107.L041302](https://doi.org/10.1103/PhysRevD.107.L041302)
- [36] Eskilt, J. R., Herold, L., Komatsu, E., Murai, K., Namikawa, T., & Naokawa, F. Constraint on Early Dark Energy from Isotropic Cosmic Birefringence. 2023, <https://arxiv.org/abs/2303.15369>
- [37] Stevens, J., Khoraminezhad, H., & Saito, S. Constraining the spatial curvature with cosmic expansion history in a cosmological model with a non-standard sound horizon. 2023, JCAP, 07, 046, doi: [10.1088/1475-7516/2023/07/046](https://doi.org/10.1088/1475-7516/2023/07/046)
- [38] Smith, T. L., & Schöneberg, N. Predictions for new physics in the CMB damping tail. 2025, <https://arxiv.org/abs/2503.20002>
- [39] Smith, T. L., Poulin, V., & Amin, M. A. Oscillating scalar fields and the Hubble tension: a resolution with novel signatures. 2020, Phys. Rev. D, 101, 063523, doi: [10.1103/PhysRevD.101.063523](https://doi.org/10.1103/PhysRevD.101.063523)
- [40] McDonough, E., & Scalisi, M. Towards Early Dark Energy in string theory. 2023, JHEP, 10, 118, doi: [10.1007/JHEP10\(2023\)118](https://doi.org/10.1007/JHEP10(2023)118)
- [41] Cicoli, M., Licheri, M., Mahanta, R., McDonough, E., Pedro, F. G., & Scalisi, M. Early Dark Energy in Type IIB String Theory. 2023, JHEP, 06, 052, doi: [10.1007/JHEP06\(2023\)052](https://doi.org/10.1007/JHEP06(2023)052)
- [42] Smith, T. L., Lucca, M., Poulin, V., Abellan, G. F., Balkenhol, L., Benabed, K., Galli, S., & Murgia, R. Hints of early dark energy in Planck, SPT, and ACT data: New physics or systematics? 2022, Phys. Rev. D, 106, 043526, doi: [10.1103/PhysRevD.106.043526](https://doi.org/10.1103/PhysRevD.106.043526)
- [43] Hill, J. C., et al. Atacama Cosmology Telescope: Constraints on prerecombination early dark energy. 2022, Phys. Rev. D, 105, 123536, doi: [10.1103/PhysRevD.105.123536](https://doi.org/10.1103/PhysRevD.105.123536)
- [44] Hill, J. C., McDonough, E., Toomey, M. W., & Alexander, S. Early dark energy does not restore cosmological concordance. 2020, Phys. Rev. D, 102, 043507, doi: [10.1103/PhysRevD.102.043507](https://doi.org/10.1103/PhysRevD.102.043507)
- [45] Raveri, M., & Doux, C. Non-Gaussian estimates of tensions in cosmological parameters. 2021, Phys. Rev. D, 104, 043504, doi: [10.1103/PhysRevD.104.043504](https://doi.org/10.1103/PhysRevD.104.043504)
- [46] Leizerovich, M., Landau, S. J., & Scóccola, C. G. Tensions in cosmology: a discussion of statistical tools to determine inconsistencies. 2023, <https://arxiv.org/abs/2312.08542>
- [47] Raveri, M., & Hu, W. Concordance and Discordance in Cosmology. 2019, Phys. Rev. D, 99, 043506, doi: [10.1103/PhysRevD.99.043506](https://doi.org/10.1103/PhysRevD.99.043506)
- [48] Efstathiou, G., Rosenberg, E., & Poulin, V. Improved Planck Constraints on Axionlike Early Dark Energy as a Resolution of the Hubble Tension. 2024, Phys. Rev. Lett., 132, 221002, doi: [10.1103/PhysRevLett.132.221002](https://doi.org/10.1103/PhysRevLett.132.221002)
- [49] Akaike, H. A new look at the statistical model

- identification. 1974, IEEE Transactions on Automatic Control, 19, 716, doi: [10.1109/TAC.1974.1100705](https://doi.org/10.1109/TAC.1974.1100705)
- [50] Andreon, S., & Weaver, B. 2015, Bayesian Methods for the Physical Sciences Learning from Examples in Astronomy and Physics (Springer Series in Astrostatistics)
- [51] Jeffreys, H. 1939, Theory of Probability (Oxford, England)
- [52] Nesseris, S., & Garcia-Bellido, J. Is the Jeffreys' scale a reliable tool for Bayesian model comparison in cosmology? 2013, JCAP, 08, 036, doi: [10.1088/1475-7516/2013/08/036](https://doi.org/10.1088/1475-7516/2013/08/036)
- [53] Smith, T. L., Poulin, V., Bernal, J. L., Boddy, K. K., Kamionkowski, M., & Murgia, R. Early dark energy is not excluded by current large-scale structure data. 2021, Phys. Rev. D, 103, 123542, doi: [10.1103/PhysRevD.103.123542](https://doi.org/10.1103/PhysRevD.103.123542)
- [54] La Posta, A., Louis, T., Garrido, X., & Hill, J. C. Constraints on prerecombination early dark energy from SPT-3G public data. 2022, Phys. Rev. D, 105, 083519, doi: [10.1103/PhysRevD.105.083519](https://doi.org/10.1103/PhysRevD.105.083519)
- [55] Feldman, G. J., & Cousins, R. D. A Unified approach to the classical statistical analysis of small signals. 1998, Phys. Rev. D, 57, 3873, doi: [10.1103/PhysRevD.57.3873](https://doi.org/10.1103/PhysRevD.57.3873)
- [56] Poulin, V., Smith, T. L., Grin, D., Karwal, T., & Kamionkowski, M. Cosmological implications of ultralight axionlike fields. 2018, Phys. Rev. D, 98, 083525, doi: [10.1103/PhysRevD.98.083525](https://doi.org/10.1103/PhysRevD.98.083525)
- [57] Lesgourgues, J. The Cosmic Linear Anisotropy Solving System (CLASS) I: Overview. 2011. <https://arxiv.org/abs/1104.2932>
- [58] Blas, D., Lesgourgues, J., & Tram, T. The Cosmic Linear Anisotropy Solving System (CLASS) II: Approximation schemes. 2011, JCAP, 07, 034, doi: [10.1088/1475-7516/2011/07/034](https://doi.org/10.1088/1475-7516/2011/07/034)
- [59] Torrado, J., & Lewis, A. Cobaya: Code for Bayesian Analysis of hierarchical physical models. 2021, JCAP, 05, 057, doi: [10.1088/1475-7516/2021/05/057](https://doi.org/10.1088/1475-7516/2021/05/057)
- [60] Torrado, J., & Lewis, A. Cobaya: code for Bayesian analysis of hierarchical physical models. 2021, JCAP, 2021, 057, doi: [10.1088/1475-7516/2021/05/057](https://doi.org/10.1088/1475-7516/2021/05/057)
- [61] —. 2019, Cobaya: Bayesian analysis in cosmology, Astrophysics Source Code Library, record ascl:1910.019. <http://ascl.net/1910.019>
- [62] Hastings, W. K. Monte Carlo Sampling Methods Using Markov Chains and Their Applications. 1970, Biometrika, 57, 97. <http://www.jstor.org/stable/2334940>
- [63] Metropolis, N., Rosenbluth, A. W., Rosenbluth, M. N., Teller, A. H., & Teller, E. Equation of State Calculations by Fast Computing Machines. 1953, Journal of Chemical Physics, 21, 1087, doi: [10.1063/1.1699114](https://doi.org/10.1063/1.1699114)
- [64] Gelman, A., & Rubin, D. B. Inference from Iterative Simulation Using Multiple Sequences. 1992, Statistical Science, 7, 457. <http://www.jstor.org/stable/2246093>
- [65] Cartis, C., Fiala, J., Marteau, B., & Roberts, L. Improving the Flexibility and Robustness of Model-Based Derivative-Free Optimization Solvers. 2018, arXiv e-prints, arXiv:1804.00154, doi: [10.48550/arXiv.1804.00154](https://doi.org/10.48550/arXiv.1804.00154)
- [66] Cartis, C., Roberts, L., & Sheridan-Methven, O. Escaping local minima with derivative-free methods: a numerical investigation. 2018, arXiv e-prints, arXiv:1812.11343, doi: [10.48550/arXiv.1812.11343](https://doi.org/10.48550/arXiv.1812.11343)
- [67] Günther, S., Balkenhol, L., Fidler, C., Khalife, A. R., Lesgourgues, J., Mosbech, M. R., & Sharma, R. K. OLÉ—Online Learning Emulation in Cosmology. 2025. <https://arxiv.org/abs/2503.13183>
- [68] Planck Collaboration, Akrami, Y., Andersen, K. J., et al. Planck intermediate results - LVII. Joint Planck LFI and HFI data processing. 2020, A&A, 643, A42, doi: [10.1051/0004-6361/202038073](https://doi.org/10.1051/0004-6361/202038073)
- [69] Balkenhol, L., Trendafilova, C., Benabed, K., & Galli, S. candl: cosmic microwave background analysis with a differentiable likelihood. 2024, Astron. Astrophys., 686, A10, doi: [10.1051/0004-6361/202449432](https://doi.org/10.1051/0004-6361/202449432)
- [70] Aghanim, N., et al. Planck 2018 results. V. CMB power spectra and likelihoods. 2020, Astron. Astrophys., 641, A5, doi: [10.1051/0004-6361/201936386](https://doi.org/10.1051/0004-6361/201936386)
- [71] —. Planck 2018 results. I. Overview and the cosmological legacy of Planck. 2020, Astron. Astrophys., 641, A1, doi: [10.1051/0004-6361/201833880](https://doi.org/10.1051/0004-6361/201833880)
- [72] —. Planck 2018 results. VI. Cosmological parameters. 2020, Astron. Astrophys., 641, A6, doi: [10.1051/0004-6361/201833910](https://doi.org/10.1051/0004-6361/201833910)
- [73] Carron, J., Mirmelstein, M., & Lewis, A. CMB lensing from Planck PR4 maps. 2022, JCAP, 09, 039, doi: [10.1088/1475-7516/2022/09/039](https://doi.org/10.1088/1475-7516/2022/09/039)
- [74] Louis, T., et al. The Atacama Cosmology Telescope: DR6 Power Spectra, Likelihoods and Λ CDM Parameters. 2025. <https://arxiv.org/abs/2503.14452>
- [75] Qu, F. J., et al. The Atacama Cosmology Telescope: A Measurement of the DR6 CMB Lensing Power Spectrum and Its Implications for Structure Growth. 2024, Astrophys. J., 962, 112, doi: [10.3847/1538-4357/acfe06](https://doi.org/10.3847/1538-4357/acfe06)
- [76] Madhavacheril, M. S., et al. The Atacama Cosmology Telescope: DR6 Gravitational Lensing Map and Cosmological Parameters. 2024, Astrophys. J., 962, 113, doi: [10.3847/1538-4357/acff5f](https://doi.org/10.3847/1538-4357/acff5f)
- [77] Eisenstein, D. J., & Hu, W. Baryonic features in the matter transfer function. 1998, Astrophys. J., 496, 605, doi: [10.1086/305424](https://doi.org/10.1086/305424)
- [78] Hu, W., & Sugiyama, N. Small scale cosmological perturbations: An Analytic approach. 1996, Astrophys. J., 471, 542, doi: [10.1086/177989](https://doi.org/10.1086/177989)
- [79] Rosenberg, E., Gratton, S., & Efstathiou, G. CMB power spectra and cosmological parameters from Planck PR4 with CamSpec. 2022, Mon. Not. Roy. Astron. Soc., 517, 4620, doi: [10.1093/mnras/stac2744](https://doi.org/10.1093/mnras/stac2744)
- [80] Pagano, L., Delouis, J. M., Mottet, S., Puget, J. L., & Vibert, L. Reionization optical depth determination from Planck HFI data with ten percent accuracy. 2020, Astron. Astrophys., 635, A99, doi: [10.1051/0004-6361/201936630](https://doi.org/10.1051/0004-6361/201936630)
- [81] Uzan, J.-P. Varying Constants, Gravitation and Cosmology. 2011, Living Rev. Rel., 14, 2, doi: [10.12942/lrr-2011-2](https://doi.org/10.12942/lrr-2011-2)
- [82] Ade, P. A. R., et al. Planck intermediate results - XXIV. Constraints on variations in fundamental constants. 2015, Astron. Astrophys., 580, A22, doi: [10.1051/0004-6361/201424496](https://doi.org/10.1051/0004-6361/201424496)
- [83] Hart, L., & Chluba, J. New constraints on time-dependent variations of fundamental constants using Planck data. 2018, Mon. Not. Roy. Astron. Soc., 474, 1850, doi: [10.1093/mnras/stx2783](https://doi.org/10.1093/mnras/stx2783)
- [84] —. Updated fundamental constant constraints from Planck 2018 data and possible relations to the Hubble tension. 2020, Mon. Not. Roy. Astron. Soc., 493, 3255,

- doi: [10.1093/mnras/staa412](https://arxiv.org/abs/10.1093/mnras/staa412)
- [85] Poulin, V., Smith, T. L., Calderón, R., & Simon, T. Impact of ACT DR6 and DESI DR2 for Early Dark Energy and the Hubble tension. 2025. <https://arxiv.org/abs/2505.08051>
 - [86] Brout, D., et al. The Pantheon+ Analysis: Cosmological Constraints. 2022, *Astrophys. J.*, 938, 110, doi: [10.3847/1538-4357/ac8e04](https://doi.org/10.3847/1538-4357/ac8e04)
 - [87] Abitbol, M., et al. The Simons Observatory: Science Goals and Forecasts for the Enhanced Large Aperture Telescope. 2025. <https://arxiv.org/abs/2503.00636>
 - [88] van der Walt, S., Colbert, S. C., & Varoquaux, G. The NumPy Array: A Structure for Efficient Numerical Computation. 2011, *Computing in Science & Engineering*, 13, 22, doi: [10.1109/MCSE.2011.37](https://doi.org/10.1109/MCSE.2011.37)
 - [89] Virtanen, P., Gommers, R., Oliphant, T. E., et al. SciPy 1.0: Fundamental Algorithms for Scientific Computing in Python. 2020, *Nature Methods*, 17, 261, doi: <https://doi.org/10.1038/s41592-019-0686-2>
 - [90] Hunter, J. D. Matplotlib: A 2D Graphics Environment. 2007, *Computing in Science and Engineering*, 9, 90, doi: [10.1109/MCSE.2007.55](https://doi.org/10.1109/MCSE.2007.55)
 - [91] Lewis, A. GetDist: a Python package for analysing Monte Carlo samples. 2019. <https://arxiv.org/abs/1910.13970>